Joint Pathology Center
Veterinary Pathology Services

WEDNESDAY SLIDE CONFERENCE 2024-2025

Conference #5 — 11 September 2024

CASE I:

Signalment:
Six years-old male common woolly monkey (*Lagothrix lagotricha*).

History:
The animal was housed at the BH-ZOO (Belo Horizonte, Brazil) and developed acute lethargy, with hypoglycemia, apathy, and hypothermia. Ultrasound examination demonstrated abundant fluid in the abdominal cavity. The animal was treated with therapeutic dos-es of ceftriaxone, dexamethasone, and mor-phine, but did not respond to treatment and died two days later.

Gross Pathology:
There was abundant yellow fibrinous exudate in the peritoneal cavity, with multifocal to coalescent hemorrhage on the serosa. Gastric and intestinal serosae had multiple red, firms, nodules ranging from 0.1 to 0.2 cm in diameter. The gastric mucosa had multifocal ulcerations with approximately 0.2 cm in diameter. There were multiple areas of fibrinous adhesion between intestinal loops, associated with a necrotic area in the jejunum. The intestinal mucosa had moderate multifocal hemorrhage. There were also multifocal hemorrhages on the mucosa of the urinary bladder. Thoracic cavity and pericardial sac had moderate amounts of translucent fluid with a small amount of fibrin. The lungs had a smooth shiny red surface, with atelectasis in left and right cranial lobes.

Figure 1-1. Abdominal viscera, woolly monkey. There is abundant yellow fibrinous exudate in the peritoneal cavity, with multifocal to coalescent hemorrhage on the serosa, (*Photo courtesy of:* Departamento de Clínica e Cirurgia Veterinária, Escola de Veterinária, Universidade Federal de Minas Gerais, Av. Presidente Antônio Carlos, 6627 – CEP 30161-970, Belo Horizonte, MG, Brazil. www.vet.ufmg.br)

Laboratory Results:
Swabs of peritoneal cavity were plated on Muller-Hinton agar (Difco, USA) supplemented with 5% equine blood, mannitol salt agar (Kasvi, Brazil), and MacConkey agar (Kasvi, Brazil), followed by aerobic incubation at 37ºC for 48 h. Colonies were subjected to matrix-assisted laser desorp-tion/ionization time-of-flight (MALDI-TOF, Bruker Daltonics) mass spectrometry with results compatible with E. coli. The E. coli isolate was positive for several virulence fac-tors encoding genes: fimH, focG, papC, papG, sfaS, cnf1, usp, hlyA, iutA, and traT. No other bacteria were isolated.

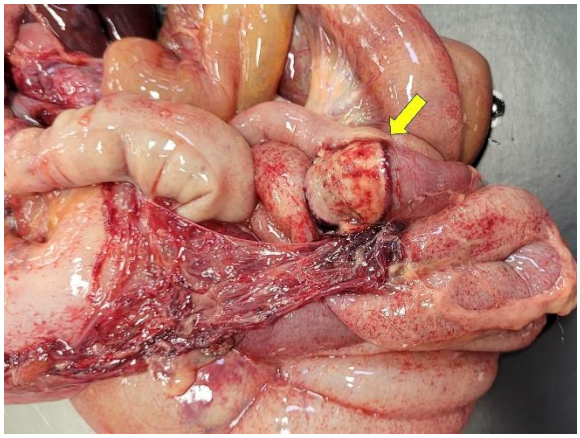

Figure 1-2. Abdominal viscera, woolly monkey. There are multiple areas of fibrinous adhesion between intestinal loops, associated with a necrotic area in the jejunum (*Photo courtesy of:* Departamento de Clínica e Cirurgia Veterinária, Escola de Veterinária, Universidade Federal de Minas Gerais, Av. Presidente Antônio Carlos, 6627 – CEP 30161-970, Belo Horizonte, MG, Brazil. www.vet.ufmg.br)

Samples of liver and spleen tested negative for yellow fever virus and dengue virus infections by RT-qPCR.

Microscopic Description:

Large intestine: submucosa was expanded with small to medium sized arteries exhibiting variable degrees of inflammation, characterized by infiltration of the tunica adventitia and media with small to moderate numbers of lymphocytes, histiocytes, neutrophils, and some plasma cells. Some of the affected vessels had proliferation of fusi-form cells with a small amount of extracellular mucinous matrix within the intima and marked accumulation of collagen in the tunica media and adventitia. Picrosirius red stained sections examined under polarized light demonstrated predominantly reddish birefringent mature type I collagen. Macrophages rich in intracytoplasmic brown pigment (suggestive of hemosiderin) were observed adjacent some of these vessels. In some sections there was marked arterial fibrinoid necrosis affecting the tunica media, often associated with thrombosis. Distribution of arterial lesions was random and segmental. The muscular layer adjacent to the areas of vascular lesion had moderate myocyte hypotrophy. Serosa had a diffuse and moderate inflammatory infiltrate, composed mainly by neutrophils, and the mesothelial cells were diffusely hypertrophic with deposition of moderate amount of fibrin at the serosa associated with neutrophils and histiocytes (peritonitis). Additionally, it was observed a moderate focally extensive area of hemorrhage at the mucosa.

Testis: similar vascular changes were observed in the testis. In addition, seminiferous tubules were marked degenerate with vacuolated Sertoli cells, thickened basal membrane and some sclerotic tubules. Diffusely, there was moderate interstitial infiltrate composed mainly by lymphocytes, histiocytes and plasma cells.

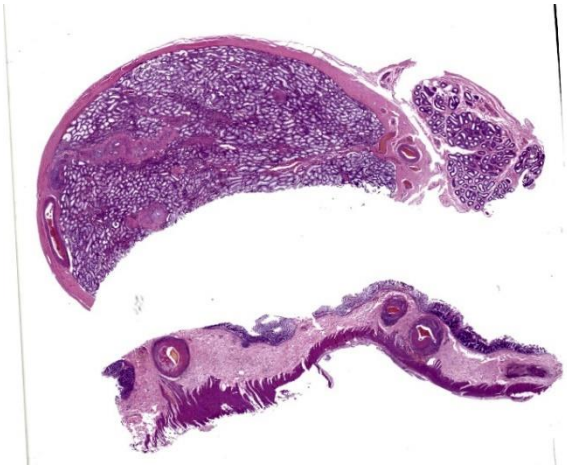

Figure 1-3. Testis and colon, woolly monkey. One section of testis (top) and colon (bottom) are submitted for examination. At this magnification, enlarged arterioles are visible within the submucosa. (HE, 6X)

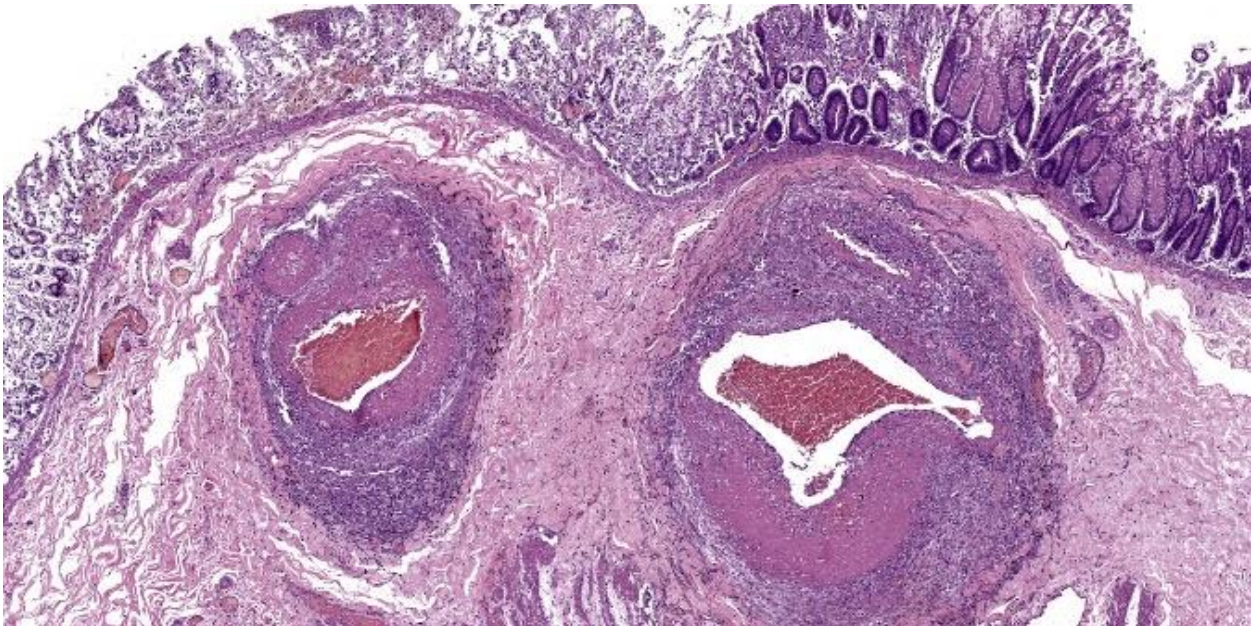

Figure 1-4. Colon, woolly monkey. The mural architecture of colonic submucosal arterials is effaced by abundant eosinophilic protein, loss of smooth muscle, and marked adventitial inflammation. (HE, 43X)

Vascular lesions were observed also at the kidneys, small intestines and stomach. At the small intestine, vascular lesions were associated with multiple focally extensive areas of transmural necrosis. Other lesions included diffuse fibrinous peritonitis, characterized by large amounts of eosinophilic fibrinous exudate with numerous neutrophils, Gram-positive and Gram-negative coccobacilli, and a few vegetal fibers. Mild pulmonary edema was also noted.

Contributor's Morphologic Diagnoses:
Large intestine: arteritis, necrotizing and proliferative, diffuse, severe with fibrinoid necrosis, thrombosis, and fibrinous peritonitis.

Testis: 1) arteritis, necrotizing and proliferative, diffuse, severe with fibrinoid necrosis and thrombosis. 2) orchitis, lymphoplasmacytic, diffuse, moderate with tubular degeneration, diffuse, moderate.

Contributor's Comment:
Vascular lesions in this common woolly monkey were consistent with polyarteritis nodosa (PAN) affecting small to medium sized arteries in the kidney, testis, stomach, small, and large intestines. This is the first reported case of PAN in this neotropical primate species. PAN is a progressive, degenerative, inflammatory, and necrotizing disease that most commonly affects small to large arteries of the mesentery, pancreas, kidney, testis, intes-tine, and heart, as described in humans,[6,14] cynomolgus macaques, rhesus monkey, owl monkey, and pigs.[2,8,9,16] The diverse types of vascular lesions suggest that the damage is polyphasic, i.e. it occurs intermittently.[6] Alt-hough the pathogenesis of PAN is not com-pletely clear, it is considered a type III hyper-sensitivity reaction caused by deposition of antigen/antibody complexes in small arteries followed by complement activation.[9]

PAN is a systemic necrotizing vasculitis, which affects predominantly medium size arteries. It has been described in humans, oc-

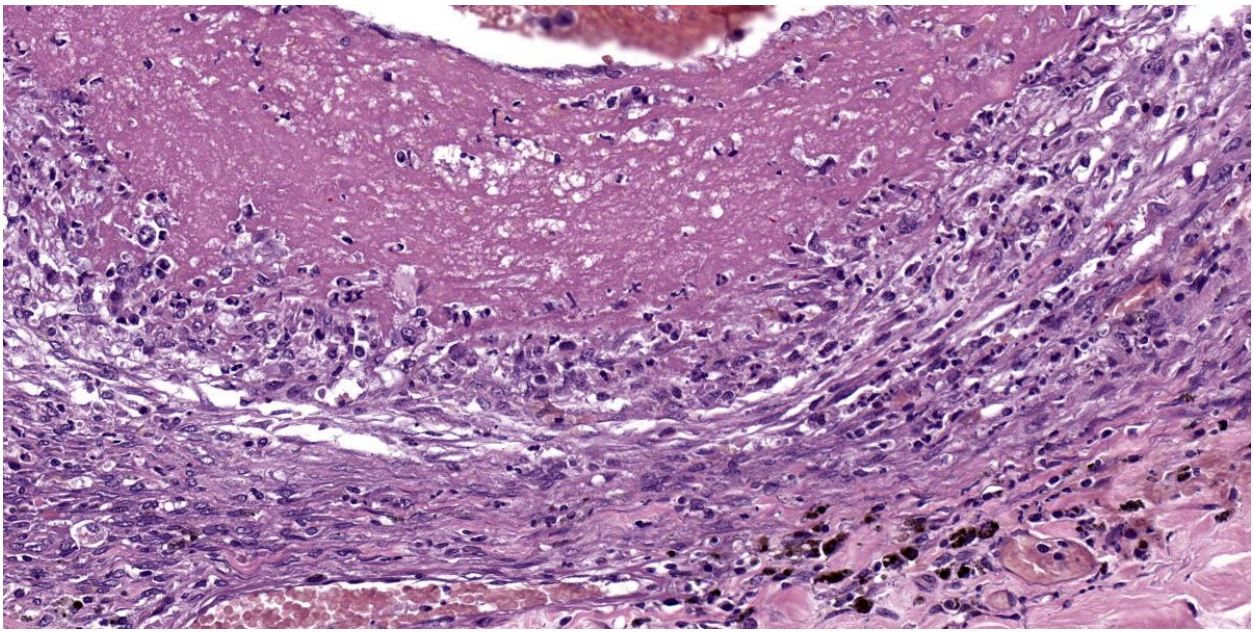

Figure 1-5. Colon, woolly monkey. The wall of an affected arteriole with the lumen at top. The media is markedly expanded by protein with necrosis and loss of smooth muscle, and marked inflammation, fibrosis, and proliferation of small vessels within the adventitia. The adjacent submucosa contains moderate numbers of siderophages. (HE, 334X)

curring more often in young adults. Small arteries may also be involved, but there is no involvement of smaller vessels, including arterioles, capillaries, and venules.[6] In animals, PAN has been reported in sheep,[15] dogs,[21] cats,[18] pigs,[12] and rats.[10] Among non-human primates, the disease has been described in cynomolgus monkey (*Macaca fasciculres*),[2,17] rhesus monkey (*Macaca mulatta*),[9] and owl monkey (*Aotus* sp.).[8]

In this case, PAN lesions were associated with transmural intestinal necrosis that resulted in peritonitis. PAN often results in narrowing of the vascular lumen due to vasculitis, with secondary gastrointestinal ulcerations or erosions due to ischemia.[1] Intestinal perforation or necrosis caused by PAN resulting in acute peritonitis has been reported in humans.[11]

Pathogenic *E. coli* was isolated from the peritoneal cavity in this case. *E. coli* is a major cause of extra-intestinal infections including meningitis, bacteremia, pyelonephritis, cystitis, prostatitis, metritis, and peritonitis.[7,20] However, it is also a member of the intestinal microbiota in mammals.[19] Extra-intestinal pathogenic *E. coli* and commensal *E. coli* typically differ in virulence factors.[7,20] In this case, the *E. coli* isolate was positive for several virulence factors encoding genes: *fimH, focG, papC, papG, sfaS, cnf1, usp, hlyA, iutA,* and *traT*.

In conclusion, this is a case of PAN associated with transmural intestinal necrosis and lethal septic peritonitis in a common woolly monkey, which has been recently published.[3] Therefore, PAN must be considered for the differential diagnosis of inflammatory, necrotizing and/or proliferative multi-systemic segmental arterial lesions in neotropical primates.

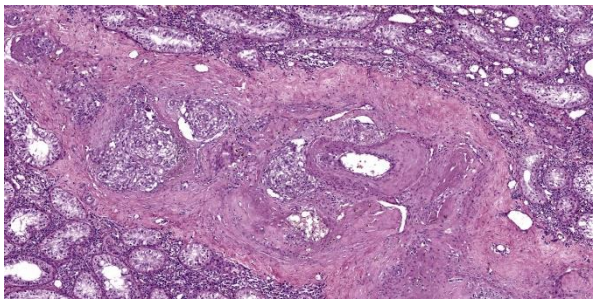

Figure 1-6. Testis, woolly monkey. Similar changes are present within the arterioles of the testis. There is atrophy of the seminiferous tubules and mild lympoplasmacytic orchitis. (HE, 75X)

Contributing Institution:
Departamento de Clínica e Cirurgia Veterinária, Escola de Veterinária, Universidade Federal de Minas Gerais, Av. Presidente Antônio Carlos, 6627 – CEP 30161-970, Belo Horizonte, MG, Brazil. www.vet.ufmg.br

JPC Diagnoses:
Colon and testis: Arteritis, proliferative, necrotizing, fibronous, chronic, multifocal, severe.

Testis: Orchitis, lymphoplasmacytic, chronic, multifocal, mild.

Colon: Serositis, fibrinous, subacute, diffuse, moderate.

JPC Comment:
This week's conference was moderated by Major Janas Gray, presently at the US Army Medical Research Institute of Chemical Defense (USAMRICD) in Aberdeen, Maryland. This first case is a terrific example of polyarteritis (periarteritis) nodosa (PAN). Alt-hough we have covered PAN in laboratory species before (most recently Conference 1, Case, 2018-2019 in a rat) we have also seen similar lesions in a cat (Conference 12, Case 4, 2022-2023), so this entity should be considered as a differential in any case of systemic necrotizing vasculitis. In particular, the sections of intestine and testis from this monkey feature robust infiltration of the adventitia and outer media by inflammatory cells (Figures 1-3 and 1-4).

This case is unusual in the degree of secondary changes present in which generated lengthy discussion. Conference participants largely agreed with the contributor's interpretation of the case but differed on how to best interpret the testis. Given that the arteritis was only multifocal, diffuse tubular changes were harder to support. In section, participants noted few spermatids within the epididymis as well as spermatogonia and spermatocytes within the seminiferous tubules, and coupled with the finding that this young in-dividual was entering the phase of sexual ma-turity reported in this species[15] led some participants to conclude that the testis was immature rather than senescent.

Another consideration for vascular lesions in the woolly monkey is idiopathic (essential) hypertension.[4,5] Microscopic features of this entity include hyaline arteriosclerosis with intramural deposition of amorphous, brightly eosinophilic material and hyperplastic arteriosclerosis with smooth muscle proliferation of the tunica intima and media. Small muscular arteries and arterioles are classically involved and the kidney is the principal organ, though changes in other arteries have been described. A recent case series looking at similar lesions in pygmy marmosets[4] identified a small number of non-renal, non cardio-pulmonary in the inner retina, stomach, spleen, and cerebrum. In the present case, the intact inner elastic lamina and lack of overt hyalinization are against this particular interpretation.

As a final aside for this case, PAN has been reported as a sequalae to human COVID-19 vaccination in line with the type III hypersensitivity reaction and resulting anti-gen/antibody complex pathogenesis the con-tributor lays out. Although PAN in humans has been

associated previously with hepatitis B vaccination, the production of viral protein through mRNA vaccines may inadvertently drive T-lymphocyte autoreactivity and resulting complement activation and cytokine cascade.[13]

References:

1. Agard C, Mouthon L, Mahr A, et al. Microscopic polyangiitis and polyarteritis nodosa: how and when do they start? *Arthritis Rheum*. 2003;49:709-715.
2. Albassam MA, Lillie LE, Smith GS. Asymptomatic polyarteritis in a cynomolgus monkey. *Lab Anim Sci.*1993;43:628-629.
3. Carvalho TP, Oliveira Santos D, Oliveira AR, et al. Polyarteritis nodosa in a captive common wooly monkey (*Lagothrix lagotricha*) associated with intestinal necrosis, peritonitis, and sepsis. *J Med Primatol*. 2023;52:197-200.
4. Cooley AJ, Savage A, Snowdon CT. Vascular, cardiac, and renal lesions attributed to primary systemic hypertension in western pygmy marmosets (*Cebuella pygmaea*). *Vet Pathol.* 2022; 59(2): 358-370.
5. Giddens WE, Combs CA, Smith OA, et al. Spontaneous hypertension and its sequelae in woolly monkeys (Lagothrix lagotricha). *Lab Anim Sci.* 1987;37(6):750–756.
6. Guillevin L. Polyarteritis nodosa and microscopic polyangiitis. In: Ball GV, ed. *Vasculitis.* Bridges; 2012:34-52.
7. Johnson JR, Stell AL. Extended virulence genotypes of *Escherichia coli* strains from patients with urosepsis in relation to phylogeny and host compromise. *J Infect Dis.* 2000;181:261-272.
8. Joint Pathology Center. Veterinary pathology service. In: Wednesday Slide Conference Proceedings. 2012- 2013; Conf 4, Case III, Accessed http://www.ask-jpc.org/wsco/wsc_show-case4.php?id=YzZnSjlnRzBk-TytDcE5QWm5EbUZCUT09 (Accessed 6 July 2022); 2012.
9. Joint Pathology Center. Veterinary pathology service. In: Wednesday Slide Conference Proceedings. 2016-2017; Conf 3, Case III http://www.ask-jpc.org/wsco/wsc_show-case4.php?id=SXgweHNQbEpUS2JU-UmhNcDlHelNYdz09 (Accessed 6 July 2022); 2016.
10. Lepherd ML, Schlafer DH, De Matos R, et al. Pathology in pratice. Polyarteritis nodosa. *J Am Vet Med Assoc.* 2013;243:1399-1401.
11. Levine SM, Hellmann DB, Stone JH. Gastrointestinal involvement in polyarteritis nodosa (1986-2000): presentation and outcomes in 24 patients. *Am J Med*. 2002;112:386-391.
12. Liu CH, Chiang YH, Chu RM, et al. High incidence of polyarteritis nodosa in the brains of culled sows. *J Vet Med Sci.* 2005;67:125-127.
13. Makiyama A, Abe Y, Furusawa H, Kogami M, Ando T, Tada K, Onimaru M, Ishizu A, Yamaji K, Tamura N. Polyarteritis nodosa diagnosed in a young male after COVID-19 vaccine: A case report. *Mod Rheumatol Case Rep*. 2023 Dec 29;8(1):125-132.
14. Mitchell RN, Halushka MK. Blood Vessels. Kumar V, Abbas AK, Fausto N, eds. In: *Robins and Cotran Pathologic Basis of Disease*. Elsevier, 2015;509-510.
15. Pereira T. H d. S., Mayor, P., Evangelista, J. S. A. M., Lima, A. K. F., de Andrade, R. d. S., & Monteiro, F. O. B. (2024). Reproductive physiology with emphasis on endometrial cycles of woolly and uakari monkeys—A literature review. *American Journal of Primatology*, 86, e23585.
16. Pesavento PA, Dange RB, Ferreras MC, et al. Systemic necrotizing vasculitis in sheep is associated with ovine herpesvirus 2. *Vet Pathol.* 2019;56:87-92.

17. Porter BF, Frost P, Hubbard GB. Polyarteritis nodosa in cynomolgus macaque (*Macaca fascicularis*). *Vet Pathol.* 2003;40:570-573.
18. Salvadori C, Vezzosi T, Marchetti V, et al. Polyarteritis nodosa in a cat with involvement of the central and peripheral nervous system. *J Comp Pathol.* 2019;167:6-11.
19. Selander RK, Levin BR. Genetic diversity and structure in *Escherichia coli* populations. *Science*. 1980;210:545-547.
20. Siqueira AK, Ribeiro MG, Leite DS, et al. Virulence factors in *Escherichia coli* strains isolated from urinary tract infection and pyometra cases and from feces of healthy dogs. *Res Vet Sci*. 2009;86:206-210.
21. Snyder PW, Kazacos EA, Scott-Moncrieff JC, et al. Pathologic Features of naturally occurring juvenile polyarteritis in beagle dog. *Vet Pathol.* 1995;32:337-345.

CASE II:

Signalment:
1-year-old, female Common Marmoset (*Callithrix jacchus*)

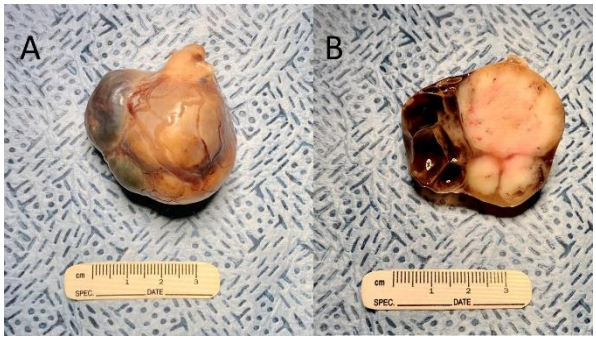

Figure 2-1. Kidney, common marmoset. A large white-tam multilobular mass is present within the kidney (intact left, cut section right) (*Photo courtesy of: Division of Laboratory Animal Resources, University of Pittsburgh. http://www.dlar.pitt.edu/)*

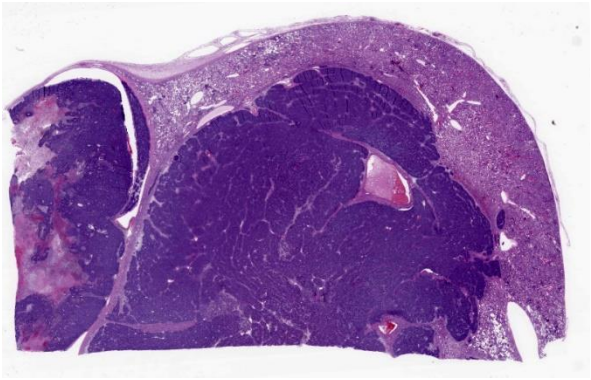

Figure 2-2. Kidney, common marmoset. Approximately 80% of the section of kidney is effaced by a neoplasm. (HE, 5X)

History:
Animal was thought to be pregnant, but ultrasound revealed a large (~5cm diameter, cystic, abdominal mass in the area of the left kidney.

Gross Pathology:
The multilobular abdominal mass enveloped the entire left kidney. On cut section, portions were white-tan and first while others were cystic and filled with yellow-brown fluid.

Microscopic Description:
Kidney: Within the cortex, compressing and effacing adjacent renal parenchyma and extending to cut borders is a mostly encapsulated, well-demarcated, lobulated, and expansile neoplasm. The neoplasm is composed of a disorganized mixture of three distinct cell populations: epithelial, mesenchymal and blastemal. In all sections, the blastemal population is the primary component and consists of polygonal cells arranged in nests sometimes separated by connective tissue. These neoplastic cells have indistinct cell borders, a small amount of eosinophilic cytoplasm and a high nuclear to cytoplasmic ratio. Nuclei are round to oval with vacuolated chromatin and indistinct nucleoli. The mitotic rate is 1 per 40x field. In some sections, these cells cant be seen within blood vessels at the periphery of

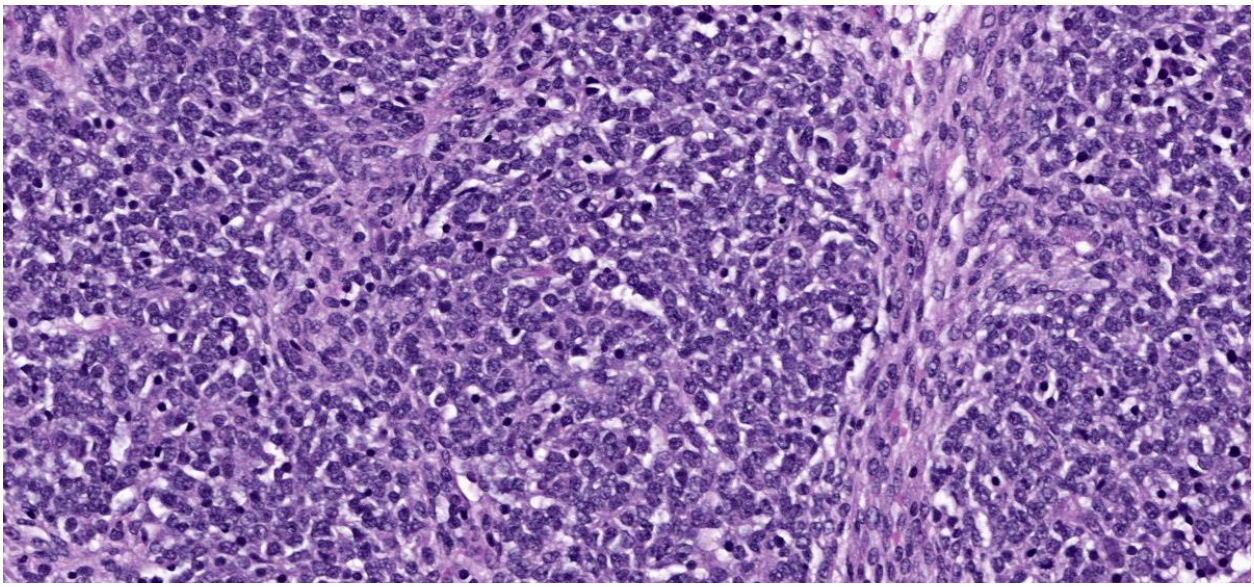

Figure 2-3. Kidney, common marmoset. The predominant cell type is a small polygonal to spindle blastemal cells which occasionally elongate forming bands of mesenchymal cells which course through the neoplasm. (HE, 315X)

the neoplasm. The epithelial population is composed of cuboidal to columnar cells arranged in irregular and often infolded tubules. Occasionally, these tubules project tufts into lumina (primitive glomeruli). These neoplastic cells have variably distinct cell borders, a moderate amount of eosinophilic fibrillar cytoplasm, round to oval nuclei, loosely clumped chromatin, and rarely contain a distinct nucleolus. The mitotic rate is 0-1 per 40x field. The mesenchymal component often blends with the other two components, and generally consists of spindle cells present within a loose, myxoid, extracellular matrix (embryonal mesenchyme). Spindle cells are stellate to spindle with indistinct cell borders, a scant amount of eosinophilic fibrillar cytoplasm, oval to elongate nuclei with finely stippled chromatin and indistinct nucleoli. The mitotic rate is <1 per 40x field. In some sections, spindle cells differentiate along the lines of cardiomyocytes characterized by elongated cells with one to several round centrally located nucleus/nuclei with vesicular chromatin and eosinophilic, crossed-striated cytoplasm containing occasional intercalated discs. Cystic areas are present in some sections of the neoplasm and are lined by attenuated epithelial cells.

Necrosis and hemorrhage are present multifocally within the neoplasm and adjacent kidney. The kidney also contains tubular atrophy and foci of mixed inflammatory cells.

Contributor's Morphologic Diagnoses:
Kidney: Nephroblastoma, Common Marmoset

Contributor's Comment:
Often called Wilms' tumor, nephroblastoma is the most common primary renal neoplasm in children, swine, chicken, and fish, the second most common primary renal tumor in cats, and the third most common in dogs.[3,10] Nephroblastoma is commonly reported in rats, and can be experimentally induced by prenatal exposure to the carcinogen N-ethylnitrosourea (ENU).[13]

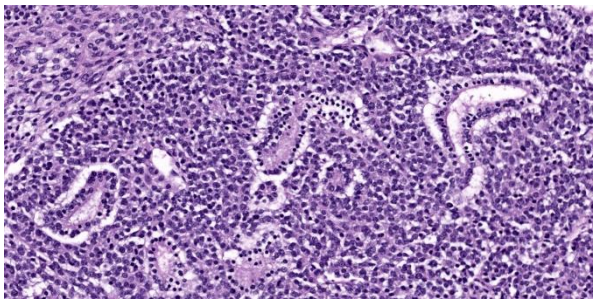

Figure 2-4. Kidney, common marmoset. Occasionally, palisading blastemal cells differentiate into tubules. (HE, 293X)

In nonhuman primates, primary neoplasms of the kidney have been reported infrequently as spontaneous cases and in association with exposure to radiation, chemical carcinogens, and parasites.[7] The most commonly described renal neoplasms in nonhuman primates include carcinomas and adenomas.[7] Only a few reports exist of nephroblastomas in Old World and New World monkeys including a report of nephroblastoma in a black-tufted marmoset[4] and a single report describing a malignant nephroblastoma in a common marmoset.[13] Interestingly, this case had similar features to that case report, including cystic areas and evidence of malignancy.

Nephroblastomas are true embryonal tumors that arise in primitive nephrogenic blastema and foci of renal dysplasia.[3] The etiology and pathogenesis of nephroblastoma has still not been fully clarified. In children, the neoplasm is frequently associated with congenital abnormalities or syndromes, including cryptorchism, hemihypertrophy, hypospadias, and sporadic aniridia. Two loci on chromosome 11, locus 11p13 (WT1 gene) and locus 11p15 (WT2 gene), have been implicated in the genesis of Wilms' tumors in children with developmental disorders. An abnormal WT1 gene is present in patients with WAGR syndrome (Wilms' tumor, aniridia, genitourinary abnormalities, mental retardation) or Denys-Drash syndrome (Wilms' tumor, progressive glomerulonephritis, male pseudohermaphroditism). A mutated WT2 gene can be observed in patients with Beckwith-Wiedemann syndrome or hemihypertrophy. However, the genetics of Wilms' tumor appear to be multifactorial and probably include further chromosomal abnormalities. Familial Wilms' tumor is rare and occurs in about 1% of cases and is not associated with mutations in chromosome 11.[1,8,13]

Contributing Institution:
Division of Laboratory Animal Resource
University of Pittsburgh
S1040 Thomas E. Starzl Biomedical Science Tower
200 Lothrop Street
Pittsburgh, PA 15261
http://www.dlar.pitt.edu/

JPC Diagnosis:
Kidney:Nephroblastoma.

Kidney: Nephritis, interstitial and lymphoplasmacytic, chronic, multifocal, mild with proteinosis.

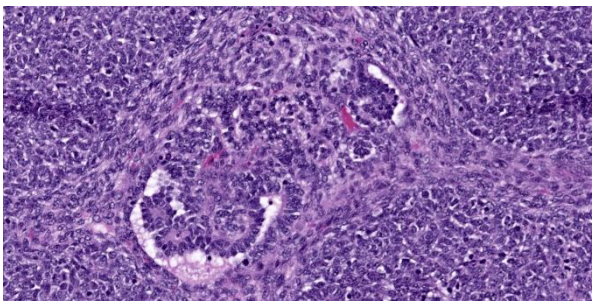

Figure 2-5. Kidney, common marmoset. Rarely, epitelial cells protrude into tubular lumina, recapitulating primitive glomeruli. (HE, 300X)

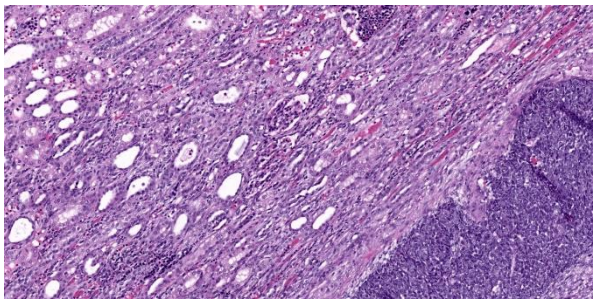

Figure 2-6. Kidney, common marmoset. At the periphery of the neoplasm, glomeruli and tubules are compressed with interstititial fibrosis. (HE, 139X)

JPC Comment:
Nephroblastoma remains a fan-favorite submission to the WSC and this case is a good example that clearly delineates the three components to describe (blastemal, mesenchymal, and epithelial) that are outlined in Figures 2-3, 2-4, and 2-5. In this case, the predominance of the blastemal cells with only rare tubular and glomerular differentiation was helpful, as trainees often have difficulty identifying blastemaConfirmatory IHCs for this case (WT1, CD56, pancytokeratin, vimentin, desmin) were not needed to arrive at the diagnosis.

Conference participants devoted a significant portion of the discussion to changes in the adjacent kidney. Participants noted occasional glomerular hypercellularity, synechiae, proteinosis, fibrosis, casts, and interstitial nephritis – we added a second morphologic diagnosis for the features we felt were best represented and not related to the neoplasm.

The constellation of glomerular changes and interstitial nephritis in this species suggests two potential concurrent pathologies. Spontaneous (chronic) progressive glomerulonephropathy (CPG) has been described previously in common marmosets[2,6,12] as has "marmoset wasting syndrome" (MWS).[9,11] Both CPG and MWS are common in this species (*Callithrix jacchus*) and can occur at any age. Additionally, both CPG and MWS cause chronic interstitial nephritis with predominantly lymphocytes and plasma cells and proteinosis as observed in this case. Low grade CPG can have subtle changes to the glomeruli, namely either hypercellularity or sclerosis of the mesangium. These changes are often absent in MWS however. In this case, we considered the possibility of low grade CPG given mildly hypercellular glomeruli with rare synechiae. In advanced cases of CPG, glomerular changes are marked and this condition can be more easily differentiated from MWS. Additionally, in cases of MWS, lymphoplasmacytic enteritis is invariably present. The presence or absence of enteric lesions was not mentioned in the clinical history, and MWS cannot be excluded as cause for the renal lesions in this case.

Finally, an important ruleout for this neoplasm is teratoma as the three cell types may be interpreted as primordial germ layers, particularly in cases where well-differentiated tissue (hair, cartilage, neural tissue, etc) is not included within the teratoma itself (see Conference 10, Case 1, 2023-2024).

References:

1. Al-Hussain T, Ali A, Akhtar M. Wilms tumor: an update. *Adv Anat Pathol*. 2014 May;21(3):166-73.
2. Brack M, Rothe H. Chronic Tubulointerstitial Nephritis and Wasting Disease in Marmosets (*Callithrix jacchus*). *Veterinary Pathology*. 1981;18(6_suppl):45-54.
3. Cianciolo RE, Mohr FC. The urinary system. In: Maxie MG, ed. *Jubb, Kennedy, and Palmer's Pathology of Domestic Animals*. Vol. 2, 6th ed. St. Louis, MO: Elsevier Limited; 2016:446-447.
4. Ferreira Junior J.A., Rissi D.R., Elias M.A., Leonardo A.S., Nascimento K.A.,Macêdo J.T.S.A. & Pedroso P.M.O. Nephroblastoma in a black-tufted marmoset (*Callithrix penicillata*). *Pesquisa Veterinária Brasileira*. 2018. 38(11):2155-2158.

5. Goens SD, Moore CM, Brasky KM, Frost PA, Leland MM, Hubbard GB. Nephroblastomatosis and nephroblastoma in nonhuman primates. *J Med Primatol*. 2005 Aug;34(4):165-70.
6. Isobe K, Adachi K, Hayashi S, et al. Spontaneous Glomerular and Tubulointerstitial Lesions in Common Marmosets (*Callithrix jacchus*). *Veterinary Pathology*. 2012;49(5):839-845.
7. Jones SR, Casey HW. Primary renal tumors in nonhuman primates. *Vet Pathol*. 1981 Apr;18(Suppl 6):89-104.
8. Lowe LH, Isuani BH, Heller RM, Stein SM, Johnson JE, Navarro OM, Hernanz-Schulman M. Pediatric renal masses: Wilms tumor and beyond. *Radiographics*. 2000 Nov-Dec;20(6):1585-603.
9. Ludlage E, Mansfield K. Clinical care and diseases of the common marmoset (*Callithrix jacchus*). Comp Med. 2003 Aug;53(4):369-82.
10. Meuten DJ, Mansfield K. Clinical care and diseases of the common marmoset (*Callithrix jacchus*). Comp Med. 2003 Aug;53(4):369-82.
11. Olstad KJ, Bleyer M. Other noninfectious conditions (inflammatory/degenerative/proliferative, immune-mediated/idiopathic/unknown in nonhuman primates. In: *Atlas of Diagnostic Pathology in Nonhuman Primates*. Kondova-Perseng I, Mansfield KG, Miller AD, editors. 211-228.
12. Yamada N, Sato J, Kanno T, Wako Y, Tsuchitani M. Morphological Study of Progressive Glomerulonephropathy in Common Marmosets (*Callithrix jacchus*). *Toxicologic Pathology*. 2013;41(8):1106-1115.
13. Zoller M, Matz-Rensing K, Fabrion A, Kaup F. Malignant nephroblastoma in a common marmoset (*Callithrix jacchus*). *Vet Pathol*. 2008:45:80-84.

CASE III:

Signalment:
7-month old, 141 kg, weaned, female, Brahman calf

History:
The calf was from the Beef Research Unit at the University of Florida (UF) composed of 237 weaned calves ranging from 6 to 8 months of age. The herd had experienced three deaths subsequent to a recent introduction of a post-weaning feed supplement to the animals. The affected calves presented with lethargy, weakness, incoordination, tachycardia, and recumbency. Clinical examination of this particular calf revealed a history of lateral recumbency and weakness within the last 24 hours, moderate dehydration, tachycardia (130 bpm), dyspnea, and ruminal hypomotility (1 weak contraction/min). The animal remained in lateral recumbency and died spontaneously within 24 hours of examination. The calf was submitted to the UF Veterinary Diagnostic Laboratories for necropsy.

Gross Pathology:
The animal was in good postmortem condition and good nutritional condition, with symmetrical muscling and appropriate subcutaneous and visceral adipose stores. Several muscle groups in the left and right thighs, especially the semimembranosus and semitendinosus muscles, contained multiple, multifocal to coalescing, ill-defined, pale tan streaks. Some skeletal muscle groups exhibited large, pale tan areas of discoloration. The superficial muscle fibers appeared more affected than the deeper ones. The pericardial sac contained mild to moderate amounts of a watery, translucent, yellow-tinged fluid. The epicardial surface of the left ventricle wall had multiple, 1-2 mm, round, flat, dark red foci. The myocardium of the left and right ventricles and interventricular septum contained multiple, multifocal to coalescing, ill-defined, pale tan streaks. The left and right cranial lung lobes

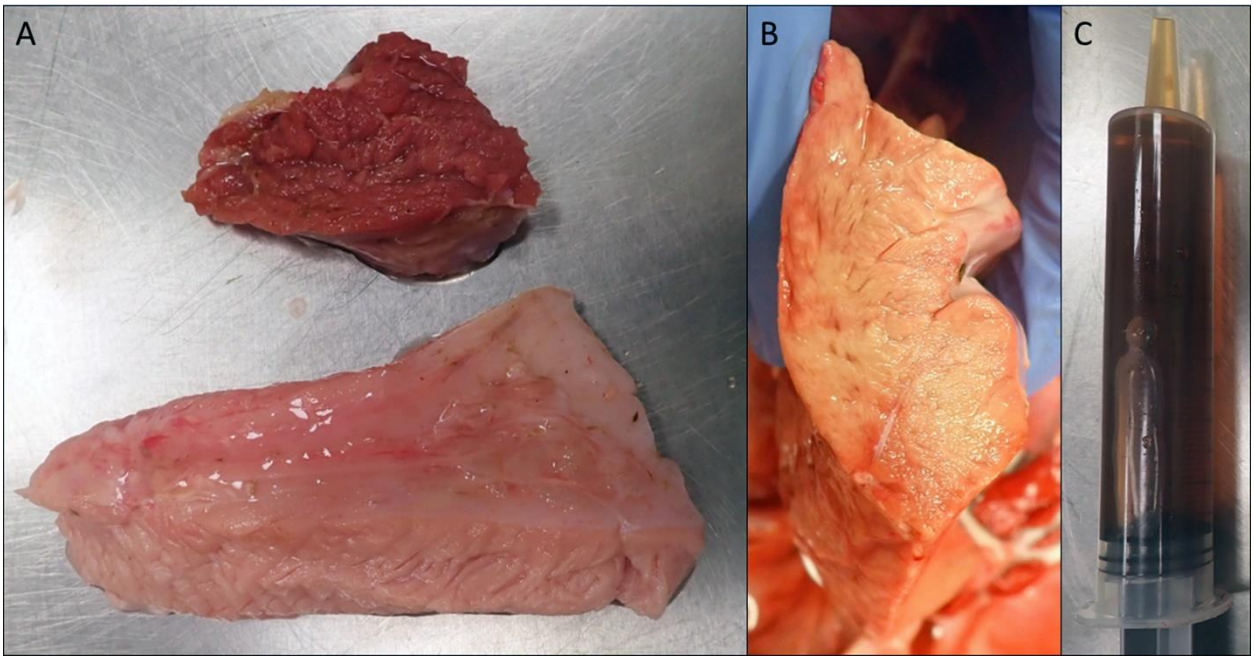

Figure 3-1. Skeletal muscle, calf. A) Some muscle groups in the thighs, especially the semimembranosus and semitendinosus muscles, exhibited large, pale tan areas of discoloration. Normal skeletal muscle at top. B) The myocardium contains multiple, ill-defined, pale tan areas of discoloration. C) Urine was dark brown. (*Photo courtesy of:* University of Florida, College of Veterinary Medicine, Department of Comparative, Diagnostic, and Population Medicine, Gainesville, Florida, USA. https://cdpm.vetmed.ufl.edu/)

had a gelatinous consistency and were mottled dark red to purple. On cut section, those lung lobes oozed a watery, translucent, red-tinged fluid. Samples of all lung lobes floated when placed in formalin. A prominent reticular pattern was observed throughout the liver lobes. The urinary bladder was distended by and filled with moderate amounts of a watery, translucent, brown-tinged fluid. No additional significant gross findings were observed in the remainder of the carcass.

Laboratory Results:

Pertinent laboratory results are indicated below.

Serum chemistry results: Creatine Kinase: 343,240 U/L; Aspartate aminotransferase: 2,335 U/L (ref: 48-139 U/L); Alkaline phosphatase: 181 U/L (ref: 30-69 U/L); Total bilirubin: 0.8 mg/dL (ref: ≤ 0.3 mg/dL); Sodium: 135.9 mEq/L (ref: 140-148 mEq/L); Calcium: 8.6 mg/dL (ref: 9.3-10.8 mEq/L); Chloride: 89.1 mEq/L (ref: 101-113 mEq/L).

Toxicology*: The levels of Monensin detected in two random samples of the feed supplement were 573 ppm and 856 ppm (Recommended label range: 11-33 ppm).

Vitamin E analysis**: The level of vitamin E detected in the submitted liver sample was 61.85 ug/g (Reference range: 7-40 ug/g)

Selenium analysis**: The level of selenium detected in the submitted liver sample was 1.31 ug/g (Reference range: 1.1-5.9 ug/g).

*Toxicology performed at the Iowa State University Veterinary Diagnostic Laboratory, Ames, Iowa

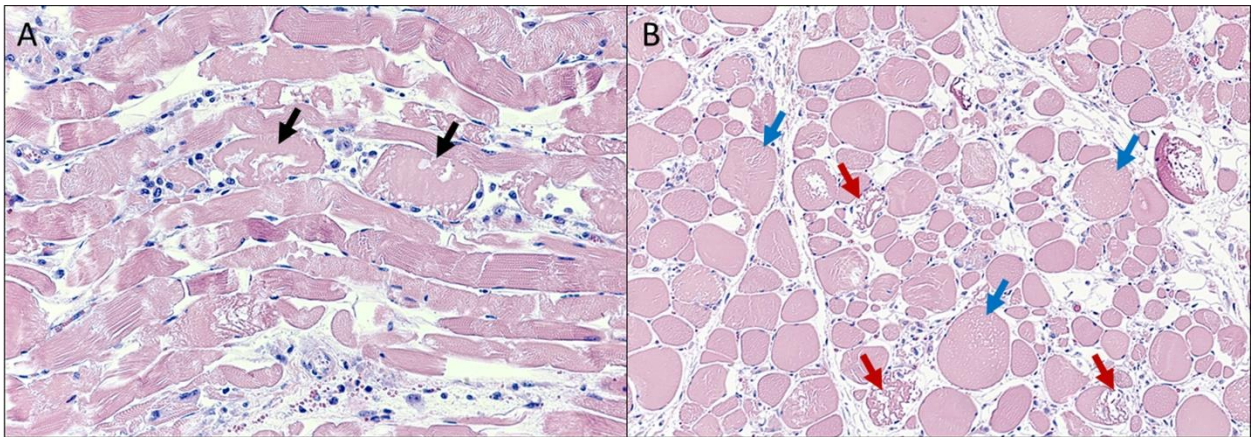

Figure 3-2. Skeletal muscle, calf. A) In longitudinal section, myofibers exhibit a hyalinized, vacuolated to fragmented sarcoplasm with loss of myofibrillar striations (black arrows). The interstitium is expanded by variable numbers of macrophages and plump, activated satellite cells (HE, 200x). B) In cross-section, myofibers were either moderately enlarged with vacuolated sarcoplasm (blue arrows) or shrunken with fragmented sarcoplasm (red arrows). Expanding the endomysium and less frequently the epimysium were small to moderate numbers of macrophages and plump satellite cells (*Photo courtesy of:* University of Florida, College of Veterinary Medicine, Department of Comparative, Diagnostic, and Population Medicine, Gainesville, Florida, USA. https://cdpm.vetmed.ufl.edu/)

**Nutrient analysis performed at the Michigan State University Veterinary Diagnostic Laboratory, Lansing, Michigan

Microscopic Description:

Skeletal muscle: Scattered throughout the musculature, myofibers are mild to moderately enlarged and have a hyalinized, often fragmented, homogeneous, eosinophilic sarcoplasm with loss of myofibrillar striations. In longitudinal sections, the myofibrils are often separated by longitudinal, empty spaces and occasionally lose their regular parallel pattern. In cross-sections, many myofibers contain variably sized, round to ovoid, empty vacuoles within the sarcoplasm. Some myofibers are shrunken, have a highly fragmented sarcoplasm, and are intermixed with pyknotic nuclei and karyorrhectic debris. Throughout the musculature, often between degenerate to necrotic myofibers are low to moderate numbers of macrophages and plump spindled cells (presumptive satellite cells).

Heart (tissue not included on the slide): The most prominent change was the presence of dense aggregates of plump, spindled cells and macrophages, replacing areas of cardiomyocyte loss. Multiple regions contain individual to small groups of cardiac myofibers with a mildly attenuated to mildly enlarged, mildly hyalinized, homogeneous, bright eosinophilic to amphophilic sarcoplasm with loss of myofibrillar striations. Often the sarcoplasm of affected myofibers is vacuolated. Occasional myofibers are hypereosinophilic with a pyknotic nucleus. Occasionally between myofibers are linear accumulations of an amphophilic granular material admixed with scant to mild amounts of karyorrhectic debris. In the interstitium, often associated with these areas and bordering myocardial vessels, are multiple, often linear, moderate density aggregates of plump spindled to stellate cells, fibroblastic cells, and macrophages. Occasionally these plump spindled cells have a large prominent nucleus with condensed, linear, deep basophilic chromatin (Anichkov cells).

Contributor's Morphologic Diagnoses:

1. Myofiber degeneration and necrosis, acute, multifocal to coalescing, marked, skeletal muscle.
2. Myocardial degeneration and necrosis, acute to subacute, multifocal, moderate, heart (tissue not included on the slide).

Contributor's Comment:

The major histopathologic changes in this calf involved several skeletal muscle groups and the myocardium, explaining clinical evidence of lethargy, weakness, and lateral recumbency noted on physical examination. Moreover, the histologic changes in the skeletal and cardiac musculatures confirm myodegeneration and myonecrosis. The widespread, synchronous muscle necrosis identified is consistent with a multifocal monophasic pattern of necrosis, suggesting a toxic myopathy or metabolic disorder[3]. Differential diagnoses for myodegeneration and myonecrosis in cattle typically include ionophore toxicosis, ingestion of myotoxic plants (e.g., *Senna* spp.), and nutritional myopathy.[1-3,7,9,13] The high serum levels of creatine phosphokinase, hepatic function dyscrasias, and hyponatremia and hypocalcemia are consistent with muscle necrosis, liver damage, and ionophore-induced influx of sodium and calcium into the cells, respectively. Pulmonary edema, pericardial effusion, and centrilobular necrosis are presumably sequelae to cardiac decompensation. A definitive cause for the cerebral vacuolar change is uncertain but may be related to tissue hypoxia/ischemia associated with cardiac failure.

In this calf, the multifocal monophasic pattern of myonecrosis, history of a newly introduced feed supplement, acute onset of clinical signs, serum chemistry abnormalities, and myocardial involvement would support the diagnosis of ionophore toxicosis.[3,4,6,13] Ultimately, this diagnosis was confirmed with the detection of toxic levels of monensin in the feed. The moderately increased levels of vitamin E in the liver and normal hepatic concentration of selenium would reduce the likelihood of nutritional myopathy as the cause of death in these calves. Furthermore, the feed and gastro-intestinal tract lacked plant parts suggestive of *Senna* spp.

Ionophore is the generic term to describe any lipid-soluble molecule that facilitates the transport of positively-charged ions across biologic membranes.[10] Monensin, lasalocid, and salinomycin are typical ionophores of veterinary clinical significance.[4,6,11,13]. Monensin is produced by the fermentation of *Streptomyces cinnamonensis*.[4,6,13] This ionophore is primarily used in veterinary medicine as an anticoccidial drug in poultry and for growth promotion and production efficiency in cattle.[4,6] Its three-dimensional (3-D) structure resembles a doughnut with the cation-binding site at the area of the doughnut hole.[10] This 3-D conformation confers some degree of selectivity for sodium and potassium to monensin.[10] The mechanism of action of monensin involves several sodium-hydrogen and potassium-hydrogen exchanges to move sodium ions into the cells and potassium ions out of the cells.[4,6,10,13]

Excessive ingestion of monensin can be toxic to several animal species. However, the susceptibility to monensin toxicosis, estimated by calculating the LD50, varies considerably among species.[3,10,14] For instance, the estimated LD50 in horses, cattle, and poultry are 2-3 mg/kg, 50-80 mg/kg, and 90-200 mg/kg, respectively, explaining why horses are very susceptible, and poultry are quite resistant to monensin toxicosis.[3,13] The pathogenesis of the disease is directly associated with the mechanism of action of monensin.[3,4,6,10,13] Long-standing, monensin-mediated accumulation of sodium into the cells, particularly myocytes and cardiomyocytes, leads to secondary water accumulation within the cytoplasm and organelles, which in turn induces

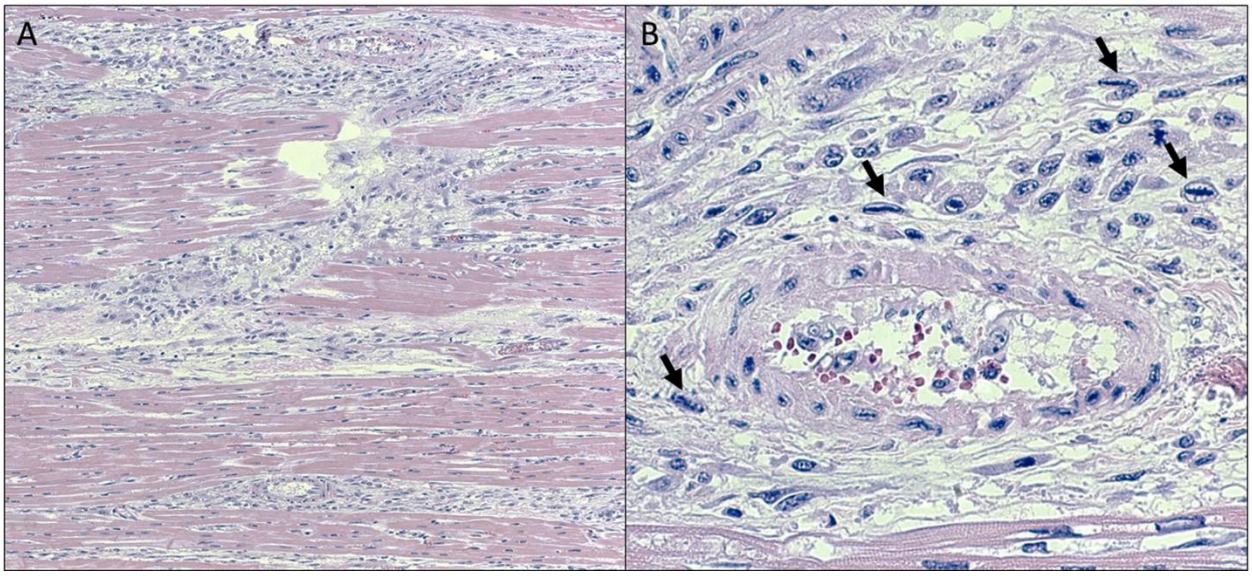

Figure 3-3. Heart, calf. A) Expanding the perimysium and replacing areas of cardiomyocyte loss are dense aggregates composed of plump spindled to stellate cells, fibroblasts, and macrophages (HE, 200x). B) These plump spindled cells (black arrows) had large prominent nuclei with condensed, linear, deep basophilic chromatin (Anichkov cells or caterpillar cells) (HE, 400x). (*Photo courtesy of:* University of Florida, College of Veterinary Medicine, Department of Comparative, Diagnostic, and Population Medicine, Gainesville, Florida, USA. https://cdpm.vetmed.ufl.edu/)

cell swelling and rupture of membranes, ultimately culminating with irreversible cell injury and cell necrosis.[3,4,6,10,13] In some instances, the toxic effects of Monensin may be potentiated with certain drugs.[1,10] Cattle ingesting nontoxic levels of Monensin in feed contaminated with macrolide antibiotic residue may still develop monensin toxicosis, presumably due to delayed hepatic clearance of monensin, resulting in accumulation and subsequent toxicity.[1]

Monensin toxicosis often is associated with feed-mixing errors that result in excess levels being added to the feed or access to feed sources destined for another species.[4,6,13,14] Grossly, several muscle groups and the myocardium have variably sized, pale tan areas of discoloration, representing areas of multifocal monophasic myonecrosis histologically.[3,4] Monensin poisoning may affect animals of all age groups.[3,4,6,13] However, heavier and stronger animals are typically the first ones to perish because of the dominant behavior allowing them to ingest more of the contaminated feed. Definitive diagnosis involves the detection of toxic levels of monensin in the suspected diet and sometimes in the ruminal content.[4,6,13] The suspected feed is the preferable sample for toxicology as the concentration of monensin in the ruminal content may be lower than that of the feed ingested due to absorption and/or ruminal breakdown[4].

Cattle may accidentally ingest *Senna* spp. when grazing or consuming feed contaminated with the plant.[5,8,12,13] Although *Senna* spp. poisoning typically causes multifocal monophasic necrosis, a similar pattern of necrosis to that induced by ionophore toxicosis,[3] absence of this toxic plant in the feedlot pen and beans and/or seeds in the feed and ruminal content would disfavor *Senna* spp. poisoning. Moreover, cattle grazing forage in soils deficient in selenium and/or being offered feed with low vitamin E content may develop nu-

tritional myopathy.[3,7] This condition commonly affects young animals, up to 6 months of age, ingesting poor-quality feed.[3] Since the calf, in this case, was in a similar age group and with myodegeneration and myonecrosis, selenium/vitamin E deficiencies were considered possible differentials. However, the typical multifocal polyphasic necrosis encountered with nutritional myopathies was not seen in this case,[3] decreasing the likelihood of nutritional myopathy. The moderately elevated levels of vitamin E and normal concentration of selenium in the submitted liver sample excludes selenium and vitamin E deficiencies as the cause of myodegeneration and myonecrosis in this calf.

Interestingly, all affected animals in the herd involved lighter animals, which is not usually the case in diet-related toxic causes where dominant animals may be exposed to a higher toxin dose. However, the animals in this herd were offered feed according to the average daily intake for the group based on the average herd weight. Therefore, by potentially receiving a higher dosage of monensin for their individual weight, it is possible these lighter animals were more susceptible to toxicosis. Deaths were not observed in the herd after discontinuing the monensin-supplemented feed.

Contributing Institution:
University of Florida, College of Veterinary Medicine, Department of Comparative, Diagnostic, and Population Medicine, Gainesville, Florida, USA.
https://cdpm.vetmed.ufl.edu/

JPC Diagnoses:
Skeletal muscle, myofibers: Degeneration and necrosis, monophasic, multifocal, moderate.

JPC Comment:
This case is a good example of a monophasic myonecrosis supported by ancillary diagnostics and a comprehensive writeup from the contributor. The lesions in the submitted slides are significantly less profound than the ones photographed by the contributor, but is consistent with "real-world" lesions in many cases of ionophore toxicosis.

Conference participants offered a number of interesting causes for this case including ionophores, vitamin E / selenium deficiency (white muscle disease), trauma (e.g. downer cow, capture myopathy) and glycogenosis type II. In downer cattle, massive focal necrosis of skeletal muscle is the result of ischemia driven by marked pressure i.e. the weight of the body is sufficient to collapse both venous and arterial blood flow.[3] The section examined lacked vascular changes and significant edema that would be anticipated as part of a reperfusion syndrome however. Given that Pompe's disease (type II glycogenosis; a lysosomal storage disease) has been described in Brahman cattle as a cause of skeletal muscle dysfunction[8,11], it does merit consideration in this case. However, the underlying cause is an autosomal recessive gene defect in acid maltase (acid α-glucosidase) with the net effect being the inability to breakdown glycogen within lysosomes during normal cellular metabolism. As such, major effects are noted in glycogen-rich, glucose-dependent tissues such as the heart and CNS with cardiac dysfunction and failure being the ultimate cause of death. The major histologic feature of Pompe's disease is marked vacuolation of skeletal myocytes, cardiac myocytes, and neurons of the PNS/CNS with vacuolization representing glycogen within lysosomes than can be confirmed via periodic acid-Schiff (PAS) with diastase treatment.[8] This is not the predominant microscopic feature in this case.

References:
1. Basaraba RJ, Oehme FW, Vorhies MW, Stokka GL. Toxicosis in cattle from concurrent feeding of monensin and dried distiller's grains contaminated with

macrolide antibiotics. *Journal of Veterinary Diagnostic Investigation*, 11(1), 79-86, 1999.
2. Blanchard PC, Galey FD, Ross F, Landgraf WW, Meyer H, Spiro N. Lasalocid toxicosis in dairy calves. *Journal of Veterinary Diagnostic Investigation*, 5(2), 300-302, 1993.
3. Cooper BJ, Valentine BA. Muscle and Tendon. In: Maxie, MG. *Jubb, Kennedy, and Palmer's Pathology of Domestic Animals*. Vol 1, 6th ed. St. Louis, Missouri; Elsevier; 2016:180-182, 208, 212-216, 218-220.
4. Ensley S. Ionophore Use and Toxicosis in Cattle. *Veterinary Clinics of North America: Food Animal Practice*, 36(3), 641-652, 2020.
5. Furlan FH, Zanata C, Damasceno ES, et al. Toxic myopathy and acute hepatic necrosis in cattle caused by ingestion of *Senna obtusifolia* (sicklepod; coffee senna) in Brazil. *Toxicon*, 92, 24-30, 2014.
6. Hall JO, Ionophore use and toxicosis in cattle. *Veterinary Clinics of North America: Food Animal Practice*, 16(3), 497-509, 2000.
7. Kennedy S, Rice DA, Davidson WB. Experimental myopathy in vitamin E- and selenium-depleted calves with and without added dietary polyunsaturated fatty acids as a model for nutritional degenerative myopathy in ruminant cattle. *Research in Veterinary Science*, 43(3), 384-394, 1987.
8. Lyons RE, Johnston DJ, McGowan MR, Laing A, Robinson B, Owen H, Hill BD, Burns BM. E7 (1057ΔTA) mutation of the acidic α-glucosidase gene causes Pompe's disease in Droughtmaster cattle. *Aust Vet J*. 2017 May;95(5):138-142.
9. Nicholson SS. Southeastern plants toxic to ruminants. *Veterinary Clinics of North America: Food Animal Practice*, 27(2), 447-458, 2011.
10. Novilla MN, McClary D, Laudert SC. Ionophores. In: *Reproductive and Developmental Toxicology*, 2nd Edition. Elsevier; 2017. pp. 503-517.
11. Reichmann K, Twist J, Thistlethwaite E. (1993), Clinical, diagnostic and biochemical features of generalised glycogenosis type II in Brahman cattle. *Australian Veterinary Journal*, 70: 405-408.
12. Rissi DR, Barros CSL. Pathology in Practice. *Journal of the American Veterinary Medical Association*, 250(1), 51-53, 2017.
13. Roder JD. Ionophore toxicity and tolerance. *Veterinary Clinics of North America: Food Animal Practice*, 27(2), 305-314, 2011.
14. Silva AWO, Mendonça MFF, Freitas MD, Filho ALR, Silva RDG, Leal PV, Pimentel LA, Peixoto TC. Accidental monensin poisoning in buffaloes in Bahia, Brazil. *Pesquisa Veterinaria Brasileira*, 42:e06937, 1-9, 2022.

Figure 4-1. Cerebrum, rhesus macaque. One section of cerebrum is submitted for examination. at subgross magnification, there are extensive areas of cavitation within the subcortical white matter. (HE, 5X)

CASE IV:

Signalment:
58 month-old, female rhesus macaque (*Macaca mulatta*)

History:
A female rhesus macaque was infected intrarectally with simian-human immunodeficiency virus [SHIV]. The monkey was on treatment for chronic diarrhea. Twenty eight months after infection, the animal developed acute epistaxis, ataxia, and a left-sided head tilt. The monkey was humanely euthanized due to worsening neurologic deficits.

Gross Pathology:
The monkey was in lean body condition with adequate hydration. The right axillary lymph node and spleen were mildly enlarged. No lesions were present in the heart, lungs, liver, kidneys, gastrointestinal or reproductive tract.

Although epistaxis was not noted grossly, there was blood on the swab collected for bacterial culture.

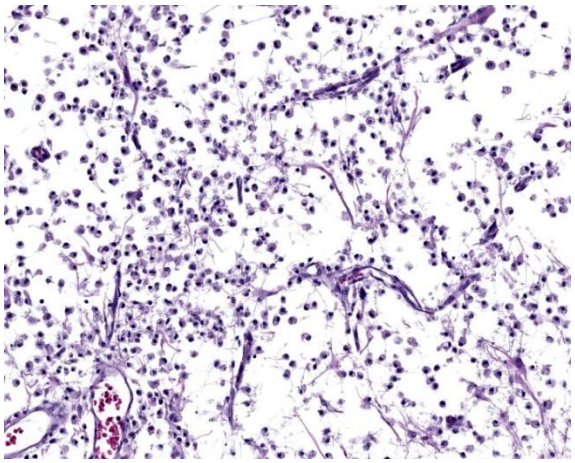

Figure 4-2. Cerebrum, rhesus macaque. Areas of cavitation contain gliovascular strands and numerous Gitter cells. (HE, 49X)

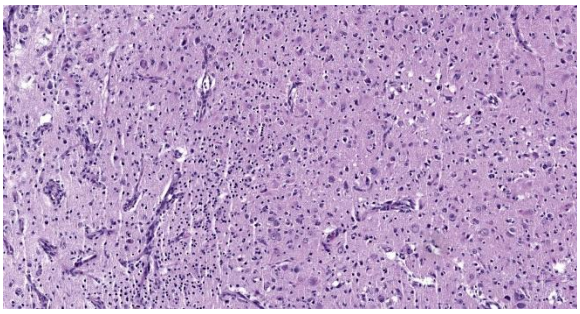

Figure 4-3. Cerebrum, rhesus macaque. Adjacent to areas of necrosis, there is marked gliosis with numerous gemistocytic astrocytes and vessels are prominent due to endothelial hypertrophy. (HE, 122X)

Laboratory Results:
Nasal culture: *Bordetella bronchiseptica*

No pathogens were noted by fecal bacterial culture. PCR results were negative for *Enterocytozoon bieneusi* and *Cryptosporidium parvum* of the liver, *Mycobacterium* sp. of the mesenteric lymph node and *Helicobacter* sp. of the stomach.

Microscopic Description:
Cerebrum: Within white matter, there is multifocal, severe parenchymal loss/cavitation with numerous central Gitter cells. Around the edges of the cavities there is marked gliosis. Oligodendrocytes are markedly enlarged, up to 5x normal, and contain variably-sized, basophilic – ground glass inclusions. Reactive(gemistocytic) astrocytes are markedly pleomorphic, bizarrely shaped, bi- or trinucleated and contain large, basophilic - ground glass inclusions. Similar astrocytes are present in the superficial cortex. Numerous vessels with markedly hypertrophic endothelial cells extend from the meninges and are present around and within the areas of cavitation. Few neutrophils and lymphocytes are present around some vessels. In the meninges, few lymphocytes, plasma cells and macrophages are present.

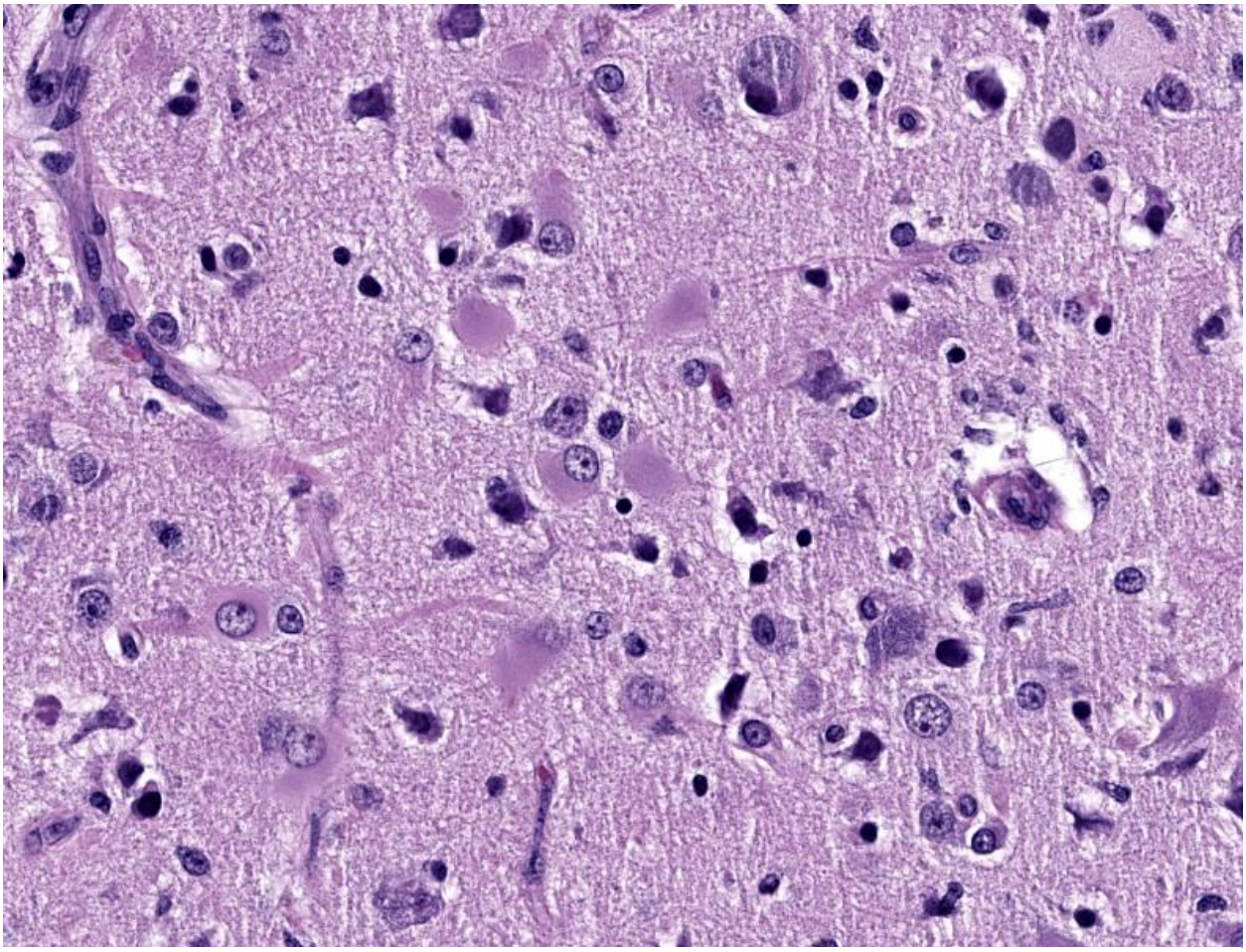

Figure 4-4. Cerebrum, rhesus macaque. High magnification of gemistocytic astrocytes in areas of gliosis. (HE, 122X)

PCR: SV40 was not detected on formalin fixed brain.

EM: Within the nucleus of oligodendrocytes, there are numerous, tightly packed, 40-45 nm viral particles arranged in paracrystalline arrays.

Contributor's Morphologic Diagnosis:
Cerebrum: Leukoencephalomalacia, severe with oligodendrocytic and astrocytic intranuclear inclusions and marked vascular hyperplasia.

Condition: Progressive multifocal leukoencephalopathy

Contributor's Comment:
SV40, Simian vacuolating virus 40, is a non-enveloped, 40 - 45nm, double stranded, circular, DNA virus of the polyomavirus family.[6,9,11] Transcription of the early regions of the viral genome produces large tumor antigen (LTag) and small tumor antigen (STag) proteins. Transcription of the late regions produces capsid proteins VP1, VP2, and VP3 and agnoprotein.[5,9,10]

Viral infection begins with VP1, VP2 and VP3 receptor mediated endocytosis.[9] Once in the nucleus, viral LTag stimulates host cell DNA synthesis and induces the cell to enter into S-phase and begin DNA synthesis. Small tumor antigen (STag) is not necessary for viral replication, but it enhances efficiency of viral replication by stimulating cells to move from G0/G1 to S phase.[10] Agnoprotein regulates viral proliferation.[5]

In addition to its capacity to cause lytic infection, SV40 LTag can cause malignant transformation by binding to and inactivating tumor suppressor proteins, retinoblastoma (pRb), p53, p107 and p130.[10] SV40 can cause tumors in vitro, or when the virus is injected into rodents or non-native hosts.[6,10,11]

SV40 is endemic in Rhesus macaques and is spread by exposure to bodily fluids such as urine or respiratory droplets. SV40 infection causes inapparent infection or mild respiratory disease or cystitis. After a period of viremia and viruria, the virus then settles in the kidneys and remains latent in immunocompetent animals.[6,11] In SIV (+) animals, virus may be found in kidney, brain, lungs and mononuclear cells.[6] Clinical disease occurs after immunosuppression due to SIV/SHIV infection, treatments with immunomodulatory medications or antirejection drugs given after experimental organ transplantation.[11-13] Clinical signs may be nonspecific, or due to other opportunistic infections, and include anorexia, diarrhea, anemia, and tissue wasting. Neurologic signs may include head tilt, ataxia, and blindness.[8] At necropsy, multifocal malacia may be visible at the junction of grey and white matter and subependymal grey matter of the cerebrum.[13]

In the CNS, two types of lesions may be found. The first resembles the changes seen in progressive multifocal leukoencephalopathy (PML) in humans. Demyelination due to infection and destruction of oligodendrocytes are found multifocally in white matter, especially at the junction with gray matter. Changes also may be found in subependymal grey matter.[6,11] Around foci of demyelination, remaining oligodendrocytes are enlarged and may contain basophilic – ground glass intranuclear inclusions. Gemistocytic astrocytes have a bizarre appearance and also may have inclusions. Numerous Gitter cells contain myelin debris.[6,11,13] The second type of lesion is meningoencephalitis of the superficial grey matter with little demyelination. In this form, inflammation expands the meninges and extends along vessels into the grey matter. More astrocytes than oligodendrocytes are affected although both cell types can have intranuclear inclusions. Vessels in affected areas have hypertrophic endothelial cells.[11,13] Both PML lesions and meningoencephalitis may be present in the same animal.[11]

In addition to the microscopic lesions in the CNS, there may be changes in the kidneys and lungs. In the kidneys, often at the corticomedullary junction, enlarged and vacuolated tubular or necrotic epithelial cells containing intranuclear inclusions along with tubulointerstitial nephritis may be present. In the lungs, there may be interstitial pneumonia with intranuclear inclusions in hypertrophic type 2 pneumocytes.[6,11-13] On electron microscopy, 45nm particles are arranged in paracrystalline arrays within the nucleus.[6]

Macaques, African green monkeys, baboons, chimpanzees, marmosets and squirrel monkeys, can be infected by polyoma virus.[11,13] Polyomaviruses in other species include:

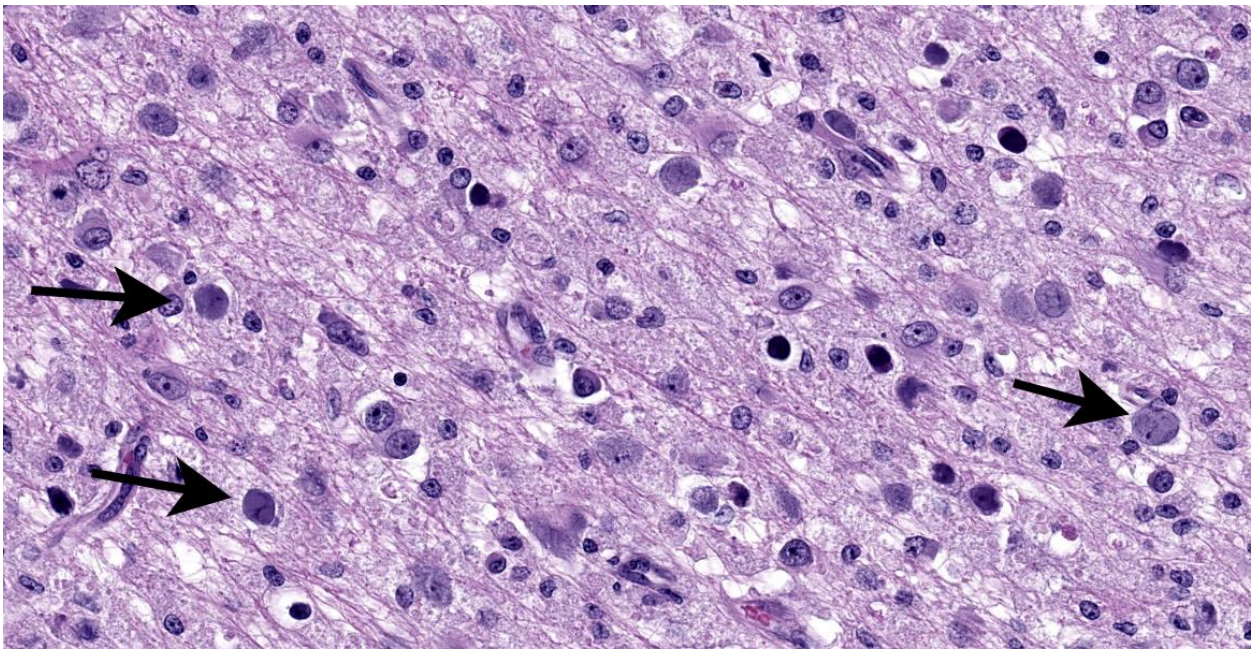

Figure 4-5. Cerebrum, rhesus macaque. Glial cells contain large amphophilic intranuclear viral inclusions (arrows). (HE, 715X)

Raccoons**:** Racoon polyomavirus: malignant peripheral nerve sheath tumors and olfactory sarcomas.[4]

Cattle: BoPy-V1, or Epsilon Polyomavirus bovis: severe tubulointerstitial nephritis with tubular epithelial cell necrosis has been reported in a fetus. However, infection in older cattle and humans has not been found to cause clinical disease.[5]

Budgerigars: Avian polyomavirus: Budgerigar fledgling disease, presents with hepatitis, ascites, and hydropericardium.[7]

Geese: Goose hemorrhagic polyoma virus: Hemorrhagic nephritis and enteritis disease, goslings die acutely with hemorrhagic nephritis and subcutaneous edema.[7]

In man, BK and JC polyomaviruses are widely spread and have a 70%-75% homology with SV40.[9,11] Most people are infected with BK and/or JC viruses in childhood and 70-90% of people are seropositive by the time they reach adulthood.[6,9,11,12] Reactivation of either virus by HIV infection, treatment with immunomodulatory drugs or immunosuppression following kidney/organ/bone marrow transplantation can lead to CNS or renal disease.[6,9] Reactivation of BK polyomavirus in kidney transplant recipients leads to nephropathy/nephritis, hemorrhagic cystitis and urethral stenosis and may lead to graft failure.[9,11,12] Reactivation of JC polyomavirus leads to progressive multifocal leukoencephalopathy characterized by demyelination with intranuclear inclusions in the oligodendrocytes. Effective treatment of HIV by antiviral medications has led to a drop of PML seen in individuals with AIDS.[9]

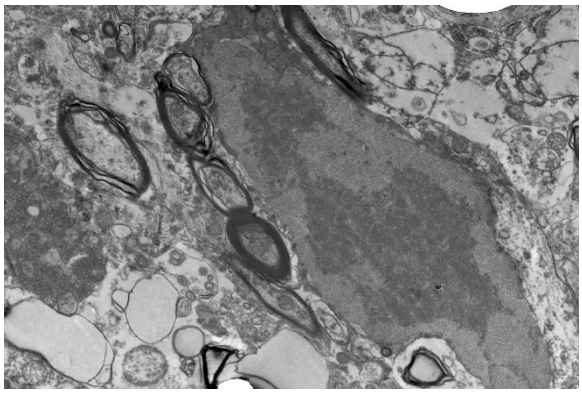

Figure 4-6. Cerebrum, rhesus macaque. Electron micrograph of a viral intranuclear inclusion in an oligodendroglial cell. (TEM, 3000X) (*Photo courtesy of:* National Institutes of Health, 9000 Rockville Pike, Bethesda, MD 20892)

Laboratory diagnosis, except for urine cytology, is based on detecting SV40 LTag, to include via PCR in CSF, urine, or sera.[3,9] Immunohistochemistry or in situ hybridization using an anti-SV40 LTag antibody can detect polyoma virus in renal or brain biopsies.[9] In urine samples, decoy cells, epithelial cells with intranuclear inclusions, and cytoplasmic fragmentation, may be used as a screening tool but inclusions due to CMV and adenovirus may look similar.[3] Progression of PML can be monitored by MRI.[1]

Polio vaccines that had been grown on rhesus kidney cell cultures and given to people from 1955 to 1963 were found to have been contaminated by SV40.[11] Due to the capacity of SV40 virus to induce malignant transformation in cell culture and cause tumors in rodents, there has been controversy over whether there has been an increased rate of cancer in people who received the contaminated vaccine. Studies have had conflicting results due to different methodologies, cross reactivity with BK and JC viruses and common seropositivity for SV40.[10,11]

Twelve new human polyoma viruses have been identified since 2007. Of the 12 new viruses, integrated BK virus has been found rarely in urological cancers. In addition, 80% of Merkel cell carcinomas, an aggressive form of skin cancer, have integrated Merkel cell polyomavirus. It may be that with newer, more sophisticated gene sequencing techniques, the association of polyomavirus and cancer may become clearer.[10]

Contributing Institution:

Matthew Starost, DVM, PhD.
National Institutes of Health
9000 Rockville Pike
Building 28A
Room 111
Bethesda, MD 20892
starostm@ors.od.nih.gov

JPC Diagnosis:

Cerebrum: Leukoencephalomalacia, multifocal to coalescing, with marked gliosis, gemistocytic astrocytosis, and glial intranuclear viral inclusions.

Cerebrum: Meningioangiomatosis, focally extensive, severe.

JPC Comment:

The contributor provides a detailed summary of SV40 that accompanies an equally impressive slide submission for this final case. We have covered SV40 leukoencephalomalacia in a rhesus macaque before (Conference 13, Case 3, 2015-2016) though this case presents outstanding histologic changes. The degree of loss of white matter (cavitation), the vascular changes, and the increased cellularity (basophilia) of the neuropil make this case almost diagnostic at subgross magnification (Figure 4-1). As the contributor notes, both oligodendro

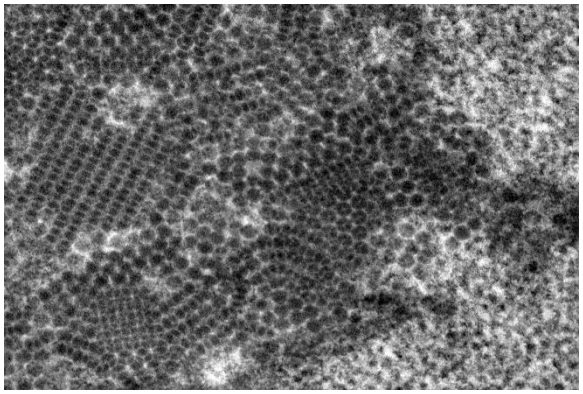

Figure 4-7. Cerebrum, rhesus macaque. Electron micrograph of a viral intranuclear inclusion in an oligodendroglial cells which demonstrates numerous icosahedral virions in paracrystalline array. (TEM, 30,000X) (*Photo courtesy of:* National Institutes of Health, 9000 Rockville Pike, Bethesda, MD 20892)

cytes and astrocytes contain characteristic intranuclear inclusions (Figure 4-5) that explain the pathogenesis of this lesion. A Luxol fast blue and modified Bielschowsky silver stain highlighted the severe loss of myelinated axons in this case. Though not particularly required at this point in lesion development, these stains may be helpful for less dramatic cases.

Conference participants were intrigued about the profound vascular changes within the cortical gray matter overlying the cavitated areas. We consulted with Dr. Andrew Miller (Cornell University) about this atypical meningovascular proliferation and ultimately decided to add a second morphologic diagnosis for this case. We excerpt his excellent commentary in part below:

"…There are 3 primary considerations for the vascular changes noted in this case. Foremost, the vasoproliferative lesion emanates from the meninges and invades into the neuroparenchyma around penetrating blood vessels and there are clearly two different cell populations present. There is one that is more spindled and likely derived from meningothelial cells and the other is blood vessels lined by reactive endothelial cells. This pattern is typical for meningioangiomatosis, though it is unlikely to be directly related to SV40 infection but instead a consequence of the profound necrosis of the underlying neuroparenchyma.

Additionally, the animal in this case was SHIV(+) and proliferative arteriopathy remains an uncommon concurrent lesion that can also been seen in SIV infection.[2] This proliferative arteriopathy can occur in a variety of organs including kidney, lung, and meningeal blood vessels where it can be associated with CNS infarction. The pathogenesis of this retroviral-associated arteriopathy is poorly understood; however, it is an important finding in a minority of SIV- and SHIV-infected macaques. That stated, these lesions are never as large or plaque-like as the area of interest in this case and typically present with single to small groups of vessels with asymmetric medial thickening, luminal narrowing, and variable thrombosis and mononuclear inflammation.[2]

Lastly, vasculitis and proliferative vascular lesions can also be associated with cytomegalovirus in immunosuppressed macaques though the large, intranuclear inclusions typical of those cases were absent in this case.[14] The lesions of this macaque do not fit the expected presentation of either retroviral-associated arteriopathy or cytomegalovirus-associated vasculitis."

References:

1. Cortese I, Reich DS, Nath A. Progressive multifocal leukoencephalopathy and the spectrum of JC virus-related disease. *Nat Rev Neurol*. 2021 Jan;17(1):37-51.
2. Chalifoux LV, Simon MA, Pauley DR, MacKey JJ, Wyand MS, Ringler DJ. Arteriopathy in macaques infected with simian immunodeficiency virus. *Lab Invest*. 1992 Sep;67(3):338-49.
3. Geetha V, Rao L, Monappa V, Susmitha M, Prabhu R. Decoy cells in urine cytology: A useful clue to post-transplant polyoma virus infection. *J Cytol*. 2012 Apr;29(2):133-4.
4. Giannitti F, Higgins RJ, Pesavento PA et al. Temporal and geographic clustering of polyomavirus-associated olfactory tumors in 10 free-ranging raccoons (Procyon lotor). *Vet Pathol*. 2014 Jul;51(4):832-45.
5. Giannitti F, da Silva Silveira C, Bullock H et al. Bovine Polyomavirus-1 (Epsilonpolyomavirus bovis): An Emerging Fetal Pathogen of Cattle That Causes Renal Lesions Resembling Polyomavirus-Associated Nephropathy of Humans. *Viruses*. 2022 Sep 14;14(9):2042.
6. Horvath CJ, Simon MA, Bergsagel DJ et al. Simian virus 40-induced disease in rhesus monkeys with simian acquired immunodeficiency syndrome. *Am J Pathol*. 1992 Jun;140(6):1431-40.
7. Johne R, Müller H. Polyomaviruses of birds: etiologic agents of inflammatory diseases in a tumor virus family. *J Virol*. 2007 Nov;81(21):11554-9.
8. Lednicky JA, Arrington AS, Stewart AR et al. Natural isolates of simian virus 40 from immunocompromised monkeys display extensive genetic heterogeneity: new implications for polyomavirus disease. *J Virol*. 1998 May;72(5):3980-90.
9. Pinto M, Pinto M, Dobson S. BK and JC virus: a review. *J Infect*. 2014 Jan;68 Suppl 1:S2-
10. Shuda, Masahiro. In: P.Boffetta and P.Hainaut, eds. Polyomaviruses in Human Cancer. *Encyclopedia of Cancer*. Vol 3, 3rd ed. Elsevier; 2019:266-27.
11. Simon MA. Polyomaviruses of nonhuman primates: implications for research. *Comp Med*. 2008 Feb;58(1):51-6.
12. Song M, Mulvihill MS, Williams KD, Collins BH, Kirk AD. Fatal SV40-associated pneumonia and nephropathy following renal allotransplantation in rhesus macaque. J *Med Primatol*. 2018 Feb;47(1):81-84.
13. Wachtman L, Mansfield K. In: C. Abee, K. Mansfield, S. Tardif, T. Morris, eds. Viral Diseases of Nonhuman Primates. *Nonhuman Primates in Biomedical Research*. Vol 2, 2nd ed. Academic Press; 2012: 25-33.
14. Yanai T, Lackner AA, Sakai H, Masegi T, Simon MA. Systemic arteriopathy in SIV-infected rhesus macaques (Macaca mulatta). *J Med Primatol*. 2006 Apr;35(2):106-12.